Journal of Materials Chemistry A

PAPER

Energy and charge transfer by donor–acceptors pairs confined in a metal–organic framework: a spectroscopic and computational investigation†

Cite this: DOI: 10.1039/c3ta14328g

Kirsty Leong,[a] Michael E. Foster,[a] Bryan M. Wong,[b] Erik D. Spoerke,[c] D. Van Gough,[c] Joseph C. Deaton[d] and Mark D. Allendorf*[a]

Received 24th October 2013
Accepted 14th January 2014

DOI: 10.1039/c3ta14328g

www.rsc.org/MaterialsA

Molecular organization of donor–acceptor pairs within a metal–organic framework (MOF) offers a new approach to improving energy and charge transfer at donor–acceptor interfaces. Here, the photophysical effects of infiltrating MOF-177 ($ZnO_4(BTB)_2$; BTB = 1,3,5-benzenetribenzoate) with α,ω-dihexylsexithiophene (DH6T) and [6,6]-phenyl-C_{61}-butyric acid methyl ester (PCBM), representing well-established polymeric and molecular materials used in organic photovoltaics, were probed using UV-visible absorption and luminescence spectroscopies combined with first-principles electronic structure calculations. The energetics of guest molecule infiltration were determined by constructing potential energy curves from self-consistent charge density-functional tight-binding (SCC-DFTB) calculations. These reveal that infiltration is energetically favored and that DH6T and PCBM are strongly bound to MOF-177 by 55 kcal mol^{-1} and 57 kcal mol^{-1}, respectively. Solution-phase infiltration with PCBM achieved a 22 wt% loading, comparable to those in bulk heterojunction solar cells, but without evidence of phase segregation. DH6T loadings were very light (maximum of ~1 molecule per 11 unit cells), but this was sufficient to produce significant quenching of the MOF-177 photoluminescence (PL). The coincident appearance of DH6T PL demonstrates that efficient Förster resonance energy transfer (FRET) from the MOF-177 linkers to DH6T occurs. These results show that the MOF is a multifunctional host that not only confines and stabilizes guest molecules, but also plays an active role, serving as a photon antenna that harvests light not efficiently absorbed by a donor molecule (DH6T in this case) and transferring it to guest acceptor molecules. Finally, time-dependent density functional theory (TDDFT) predicts the existence of linker-to-PCBM charge transfer states, suggesting that photoconductivity might be achievable in an appropriately designed guest@MOF system.

Introduction

Organic photovoltaics (OPVs) are excitonic devices in which the absorption of light by an organic semiconductor with a low dielectric constant generates bound electron–hole pairs (excitons) that are subsequently dissociated in a charge transfer (CT) event at the interface with a second, electron-accepting organic semiconductor. The mechanism of charge separation in polymeric bulk hetero-junction photovoltaic cells is described as electron transfer from the absorbing polymer to an electron acceptor *via* an excited D^+–A^- CT state,[1] potentially involving resonance energy transfer (RET) between the donor and acceptor.[2,3] Two factors limiting the performance efficiency of OPV devices are the nature of the donor–acceptor (D–A) interface and the exciton diffusion length, which in conjugated polymers is typically <10 nm before recombination occurs.[4] Much OPV research is directed toward ensuring that the D–A materials form continuous nanoscale networks within the entire photoactive layer, that their interfacial area is maximized, and that they have the proper orientation for efficient exciton splitting.[5–8] A nanoscale interpenetrating network with crystalline order of both constituents is, therefore, a desirable architecture for the active layer in photovoltaic devices.[9,10] Unfortunately, control over both the intermolecular (D–A) and meso (exciton diffusion) length scales is difficult to achieve in conventional bulk heterojunctions due to the inherent disorder of polymeric and/or molecular species in a (typically) amorphous matrix. Further complicating this situation is the need for proper alignment of the D and A electronic bands to enable efficient harvesting of the solar spectrum as well as exciton

[a]Sandia National Laboratories, Livermore, CA 94551-0969, USA. E-mail: mdallen@sandia.gov
[b]Department of Chemistry and Department of Materials Science & Engineering, Drexel University, Philadelphia, PA 19104, USA
[c]Sandia National Laboratories, Albuquerque, NM 87185-1411, USA
[d]Department of Chemistry, North Carolina State University, Raleigh, NC 27965, USA

† Electronic supplementary information (ESI) available. See DOI: 10.1039/c3ta14328g

splitting,[11] which limits further modification of the chemical structure of D and A to promote local ordering.

Metal–organic frameworks (MOFs) are crystalline nanoporous materials that offer a new approach to solving these challenging problems. MOFs are a class of hybrid supramolecular materials formed from metal cations or clusters serving as "nodes" connected to multi-topic, electron-donating organic ligands, creating ordered networks with permanent nanoporosity.[12–14] MOFs possess three critical properties relevant to controlling donor–acceptor interfaces. First, they are crystalline materials, which create a highly ordered and well-defined structure in which the position of all framework atoms is known with sub-angstrom precision. Second, they incorporate both inorganic and organic components, providing an unprecedented ability to tune the electronic structure. This also enables the pore size and chemical environment to be tailored; a number of isoreticular series are now known that enable systematic variation of structural and chemical properties.[15–17] Third, the rigid MOF structure creates permanent nano-porosity (1–10 nm diameter), which enables the fabrication of hybrid composites by filling the pores with guest molecules. Conceivably, D–A pairs could be co-located within a highly ordered, well-characterized structure. The high degree of organic linker ordering achievable within crystalline MOFs therefore provides a basis for systematically relating structure and composition to photon capture, energy transport, and delivery.[18]

The vast majority of MOFs are dielectric materials with wide band gaps.[19–22] This suggests that MOFs can serve as passive hosts to maintain close proximity and proper intermolecular alignment between donor and acceptor for efficient energy or charge transfer. In addition, however, many frameworks display linker-based luminescence,[23] enabling the framework to function as a photon antenna that increases light absorption. This concept was recently demonstrated using a pillared-paddlewheel MOF in which linker-to-linker energy transfer enabling broad coverage of the visible spectrum.[18] Lin and co-workers also reported facile intracrystal site-to-site energy migration dynamics in Ru(II)/Os(II) (2,2′-bipyridine)$_3$-based MOFs through luminescence quenching measurements.[24–26] Jin and co-workers reported an enhancement of light harvesting *via* energy transfer from QDs (coated on the surface of the framework) to the MOFs.[27] These works show the potential of appropriately designed MOFs functioning as light-harvesting and energy-transport structures.

Energy transfer involving guest molecules within the MOF pores is also feasible, as shown by Streit *et al.* using MOF thin film loaded with a europium β-diketonate complex.[28] These authors assumed that Dexter energy transfer was occurring, although no evidence for a ground-state complex required by this mechanism was provided. Nevertheless, they pointed out that efficient energy transfer by this quantum-mechanical effect requires the donor HOMO and acceptor LUMO to be energetically matched. Reasoning from these results, we hypothesized that MOFs could be used to overcome critical problems associated with the classical bulk heterojunction as a result of the following features. First, confinement within the pores allows donor–acceptor separations that are within critical distances at three key length scales important to efficient energy and/or charge transfer: (1) the exciton diffusion distance (typically ≤ 10 nm for organic materials); (2) the Förster radius for classical fluorescence resonance energy transfer (FRET; ∼ 5 nm for many fluorescent molecules); and (3) the π-stacking distance (∼3.5 Å) for Dexter energy transfer. Second, proper alignment of the donor and acceptor orbitals with the MOF band structure, which is essential for efficient energy or charge transfer regardless of the mechanism, can be achieved by tuning the MOF linker and/or metal ion. This tunability can also promote efficient use of the solar spectrum by allowing the band gap of semiconducting MOFs to be adjusted. Finally, the co-location of donor and acceptor eliminates problems associated with phase segregation, which in bulk heterojunctions reduce efficiency by creating dead ends or disordered boundaries between materials that quench excitons or trap charge.

Here, we describe an important step toward realizing the use of MOFs as components of OPV active layers, presenting spectroscopic data and electronic structure calculations demonstrating that the advantages described above can be realized using a MOF that functions as both a host for immobilizing donor and acceptor molecules and a photon antenna to scavenge and transfer energy to these guest species. As donor and acceptor we selected two molecules representative of those typically used in bulk heterojunctions: as acceptor, α,ω-dihexylsexithiophene (DH6T), a thiophene oligomer similar to the polymer P3HT, and as donor, [6,6]-phenyl-C_{61}-butyric acid methyl ester (PCBM), among the most effective acceptors used in OPV active layers. Obtaining significant loading levels with either of these large molecules requires a MOF with large pores, so we selected MOF-177, which can accommodate large polycyclic organic dye molecules and C_{60}.[29] This MOF has a 1-D channel and one unique cavity (9 : 4 ratio), labeled channel A and cavity B in Fig. 1. The diameters of these pores are approximately 14 Å for channel A and 24 Å for cavity B and can accommodate individual donor or acceptor molecules, placing them in close proximity to each other, but preventing phase

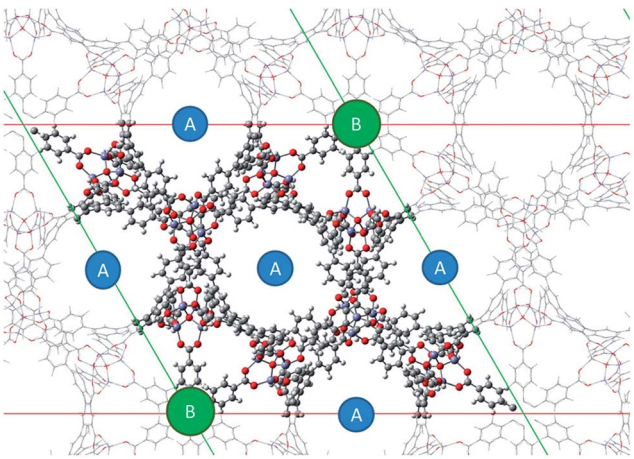

Fig. 1 DFTB+ optimized structure shows 1-D pore channel (channel A) and a cavity (cavity B) (9 : 4 ratio). The insert shows an optical image of MOF-177 crystals.

segregation. The resulting multi-molecular-MOF hybrid harvests energy and efficiently transfers it to the infiltrated molecules.

Experimental and computational methods

Electronic structure calculations

The electronic and structural properties of MOF-177 were modeled using the self-consistent charge density-functional tight-binding[30–32] (SCC-DFTB) method. The SCC-DFTB method is an approximation to Kohn–Sham density functional theory (KS-DFT) utilizing a parameterized Hamiltonian matrix; therefore, the accuracy of the method ultimately depends on the parameters (Slater–Koster files) used. This method was chosen for its balance between computational efficiency and accuracy. An efficient computational method is required to circumvent the large sizes of the MOF systems (1628+ atoms) considered which are computationally demanding for traditional DFT methods. Here, the Zn–X (X = H, C, N, O, S, and Zn)[33] and O–N–C–H[32] SCC-DFTB Slater–Koster files developed for metal–organic molecules and solids were used, which are well suited for modeling MOF-177. All SCC-DFTB calculations were carried out using the DFTB + simulation package.[34]

A geometry optimization using periodic-boundary-conditions (PBC) was carried out on MOF-177 using SCC-DFTB and employing the Lennard-Jones dispersion correction within DFTB+. During the optimization both the cell and atom positions were relaxed until a maximum force component of 0.001 a.u. was reached. A single gamma point was used for sampling the Brillouin zone during the optimization due to the large size of the unit cell. The k-space sampling was increased to a $3 \times 3 \times 3$ grid to improve the accuracy of the total and partial density-of-states (DOS). SCC-DFTB calculations were also performed on isolated PCBM and DH6T molecules in 50 $Å^3$ boxes. These calculations enable direct comparison to the MOF's electronic properties.

Potential energy curves of the infiltration of MOF-177 with PCBM and DH6T were generated to determine whether infiltration is energetically favored. For PCBM infiltration, a slab consisting of approximately 50 Å of vacuum space (total cell length of 80 Å) in the *z*-direction was created from the optimized MOF-177 unit cell. For infiltration with DH6T, which is a longer molecule than PCBM, a $1 \times 1 \times 2$ supercell slab was created with approximately 60 Å of vacuum space (total cell length of 120 Å) in the *z*-direction. To maintain proper atomic valences within the periodic slabs, the appropriate atoms were terminated with hydrogen atoms. The constructed slabs consisted of a total of 820 and 1628 atoms respectively. Finally, the atom positions within the slabs were optimized before adding the infiltrating molecule to the calculation. The centers-of mass of the infiltrating molecules were placed along an arbitrary axis passing through the small pore of MOF-177 (pore A, see Fig. 1). The molecules were then translated in increments of 1 Å and rotated around this axis in increments of 15° and 30°, generating a total of 663 and 637 starting structures mapping the infiltration of PCBM and DH6T, respectively. Ten-step geometry optimizations were performed with SCC-DFTB to remove any close contacts that might have been created.

Time-dependent density functional theory (TDDFT) was employed to probe the interactions between the organic linker (H_3BTB) and PCBM and DH6T. These calculations were carried out using the range-separated wB97xD functional[35] and the 6-31G(d,p) valence double-zeta polarized basis set. This functional is a well-tested method for capturing van der Waals interactions and long-range charge–transfer, which are essential for this system. For consistency with experiment, a polarizable continuum model (PCM) was used to incorporate solvent effects of chloroform ($\varepsilon = 11.00$). Full ground-state geometry optimizations using the respective functional were performed for all complexes, followed by TDDFT (using the linear-response formalism) calculations considering the first 100 singlet excitations. All DFT and TDDFT calculations were performed with Gaussian 09 (ref. 36) using the default convergence criteria.

MOF synthesis and infiltration

All reagents, 2,2′:5′,2″-terthiophene (3T), 3,3‴-dihexyl-2,2′:5′,2″:5″,2‴-quaterthiophene (DH-4T), and α,ω-dihexylsexithiophene (DH6T) were purchased from Sigma-Aldrich (St Louis, MO) and used as received unless stated otherwise. Phenyl-C_{61}-butyric acid methyl ester (PCBM) was purchased from American Dye Source (Quebec, Canada). Solvents used for MOF activation and exchange were stored over dried molecular sieves (4 Å).

MOF-177 was synthesized using a previously published protocol.[37] Briefly, zinc nitrate hexahydrate (0.368 g) and 4,4′,4′-benzene-1,3,5-triyl-tribenzoic acid (H_3BTB) (0.180 g) were dissolved in DEF (10 mL) in a 20 mL vial, capped tightly and heated to 100 °C for 20 hours. The solution was decanted and the crystals thoroughly washed with DMF, then exchanged with $CHCl_3$ for three days. The material was evacuated at 125 °C for 6 hours. MOF-177 crystals were infiltrated by soaking in saturated solutions of DH6T (1.0×10^{-4} M), PCBM (20 mg mL^{-1}), or a mixture of 3T, DH-4T, or DH6T + PCBM in chlorobenzene for one week. After soaking for one week, the crystals were thoroughly washed and rinsed with chlorobenzene. The solvent washings were analyzed for PCBM and DH6T using UV-vis spectroscopy; none was detected. Then the material was activated at 125 °C for 6 hours. An SEM image taken of the as-synthesized crystals show they are approximately 100–200 μm in size (see ESI, Fig. S1†).

Characterization methods

The loading of DH6T and PCBM in MOF-177 was quantified by digesting a known sample mass in a 1.0 M sodium hydroxide (NaOH) solution. DH6T and PCBM were extracted from this solution using a known volume of chlorobenzene, in which both molecules are highly soluble, which was then washed with water. The amounts of DH6T and PCBM were quantified using UV-vis spectroscopy and calibration curves obtained from known concentrations of DH6T and PCBM.

Scanning electron microscopy (SEM) was performed using a Zeiss Gemini Ultra-55 Analytical Scanning Electron Microscope with 1 nm resolution; images were collected at 30 kV.

Steady-state and time-resolved photoluminescence measurements were collected using a Horiba Jobin-Yvon Fluorolog 3-21 fluorimeter, employing a 450 W Xe arc lamp and 341 nm nanoLED, respectively. Photoluminescence experiments were conducted on crystalline powder samples of MOF contained in a powder stage holder. Absolute photoluminescence quantum yields of the crystalline MOF-177 and H_3BTB linker were measured in the integrating sphere system of a Hammamatsu Model C11347-11 Absolute Pholuminescence Quantum Yield Spectrometer. Diffuse reflectance UV-vis-NIR spectra were recorded on a Cary 5000 spectrophotometer equipped with a reflectance sphere. The Kubelka–Munk conversion, $F(R)$ *vs.* wavenumber, of the raw diffuse reflectance spectrum (R *vs.* wavenumber) was obtained by applying the formula:

$$F(R) = (1-R)^2/2R \quad (1)$$

This transform creates a linear relationship for the spectral intensity relative to sample concentration and assumes an infinitely dilute, infinitely thick sample in the non-absorbing (Spectralon) matrix, and that the sample had a constant scattering coefficient. From the diffuse reflectance spectrum, the band gap energy of MOF-177 was experimentally determined using following equation:

$$E_g = hc/l = (1240 \text{ eV nm})\ l^{-1} \quad (2)$$

where h is Planck's constant (4.13×10^{-15} eV s), c is the speed of light (2.998×10^8 m s^{-1}) and l is the absorption edge (λ in nm).

Powder X-ray diffraction experiments were carried out using a PANalytical Empyrean™ diffractometer equipped with a PIXcel-3D detector operating in scanning line detector mode with Cu K-alpha radiation ($\lambda_\alpha = 1.54187$ Å). The samples were activated and then ground to a fine powder in ambient air, applied to a low background sample holder and mounted to a flat sample stage. Raw data were then evaluated using the X'Pert HighScore Plus™ software V 3.0.0 (PANalytical, The Netherlands).

Results

Electronic structure calculations

MOF-177. Using a combination of first-principles electronic structure calculations and UV-visible spectroscopy, we confirmed that the band gap and band alignment of MOF-177 are such that neither energy nor charge transfer are feasible from infiltrated molecules to the framework. Based on SCC-DFTB calculations, the band gap of MOF-177 is predicted to be 3.35 eV, with a valence band (VB) maximum at −6.15 eV and conduction band (CB) minimum at −2.80 eV. The predicted band gap is in excellent agreement with the value of 3.3 eV which we determined by diffuse reflectance measurements, based on a band cutoff at 380 nm (ESI, Fig. S2†).

The partial density of states (PDOS) (Fig. 2) indicates that the composition of the MOF-177 band edges are dominated by the

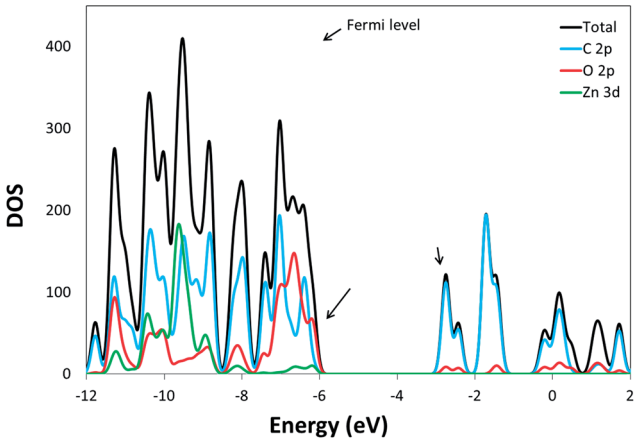

Fig. 2 Partial density of states (PDOS) – density functional tight-binding (DFTB) calculations of MOF-177.

H_3BTB linker, with minimal contribution from the zinc clusters (Zn–O). Therefore, we expect that the electronic structure of the linker governs the MOF absorption and emission properties. Steady-state luminescence spectroscopy and timing analysis of MOF-177 and the H_3BTB linker in dilute solution confirm this conclusion. As seen in Fig. 3, the excitation and emission spectra of MOF-177 are very similar to those of H_3BTB. The MOF-177 excitation and emission maxima occur at 345 and 380 nm, respectively, whereas these maxima occur at 345 nm and 390 nm for H_3BTB in dilute solution. The slight (10 nm) blue shift in the MOF-177 emission spectrum is similar to what is observed in other Zn-carboxylate MOFs.[38] The emission decay curves of MOF-177 and H_3BTB in dilute solution can both be fitted to a bi-exponential decay curve (Table 1), yielding similar average lifetimes (τ_{avg}) of 20.9 ns and 20.7 ns, respectively. This is consistent with our previous spectroscopic investigations of

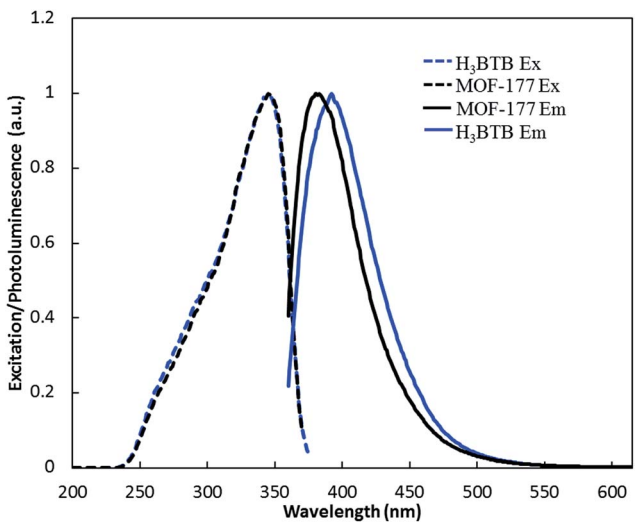

Fig. 3 Solid state excitation and emission of MOF-177 (black) and dilute solution of H_3BTB (blue) in DMF (1.0×10^{-6}M). MOF-177: $\lambda(ex)_{max} = 345$ nm; $\lambda(em)_{max} = 380$ nm. H_3BTB: $\lambda(ex)_{max} = 345$ nm; $\lambda(em)_{max} = 390$ nm.

Table 1 Solid state lifetimes of MOF-177, infiltrated MOF-177, H_3BTB, and DH6T[a]

	τ_0 (ns)	τ_1 (ns)	τ_2 (ns)	τ_{avg}
MOF-177	10 ± 0.28 (22%)	24 ± 0.09 (78%)	—	20.9
DH6T@MOF-177	8 ± 0.20 (25%)	15 ± 0.11 (75%)	—	13.3
PCBM@MOF-177	1 ± 0.04 (22%)	9 ± 0.39 (78%)	—	7.2
DH6T + PCBM@MOF-177	0.4 ± 0.001 (92%)	4 ± 0.02 (6%)	15 ± 0.72 (2%)	2.5
H_3BTB (solid)	8 ± 0.39 (10%)	17 ± 0.04 (90%)	—	16.1
H_3BTB (in DMF)	5 ± 0.32 (2%)	21 ± 0.05 (98%)	—	20.7
DH6T	0.5 ± 0.01 (87%)	2 ± 0.002 (13%)	—	0.7

[a] Average lifetimes were calculated using the equation $\tau_{avg} = \sum A_i\tau_i / \sum A_i$.

zinc-carboxylate MOFs, which indicate there is little charge transfer between the organic linker and the closed d shell of the metal ion.[38,39]

(Guest molecule)@MOF-177. SCC-DFTB calculations show that MOF-177 can accommodate both DH6T and PCBM and that infiltration is energetically very favorable, both of which agree with experimental results described in the next section. Boltzmann averages of the total energies (SCC-DFTB, see above for computational details) created upon rotation are plotted *versus* the translational increments in Fig. 4. The nature of the potential energy curves implies that the DH6T molecule, in spite of its rather large size (36.7 Å by 6.8 Å), and PCBM (11.7 Å by 12.1 Å) are capable of diffusing through the MOF pores. As the molecules enter the pore, the total energy of the system decreases, indicating that a more stable system resulted. Moreover, no indications of an energy barrier are observed upon either PCBM or DH6T entering, suggesting that infiltration is feasible. Guest molecules infiltrating MOF-177 will likely enter and travel through Channel A because the cavity of B is blocked by the H_3BTB linker (no direct route through the MOF); however, diffusion into cavity B is feasible, but expected to be less energetically favorable than traveling through channel A. The diffusion of DH6T into cavity B is not plausible due to its long chain length and rigid backbone which severely hinders its ability to make the required 90° turn. This explains the decreased loading of DH6T observed compared to PCBM.

SCC-DFTB calculations indicate that DH6T and PCBM are strongly bound within the MOF-177 pore; the predicted binding energies (total energy of the system minus the optimized energy of the slab and the isolated infiltrating species) are 55 kcal mol^{-1} and 57 kcal mol^{-1}, respectively. (Note: the predicted binding energies neglect solvent effects, therefore, the actual values may differ.) The preferred orientation of the two molecules within MOF-177 was predicted by carrying out full geometry optimizations for the structures corresponding to the energy minimum of each curve in Fig. 4b. The calculations indicate that DH6T absorbs onto the side wall of the MOF with pi–pi stacking observed between many different H_3BTB linkers. We also find that PCBM orients within the MOF between two H_3BTB linkers, such that the π orbitals of the linkers overlap with the fullerene ring of PCBM. This suggests the possibility of charge transfer between the MOF linker and PCBM, prompting us to perform time-dependent DFT (TDDFT) calculations (see ESI†).

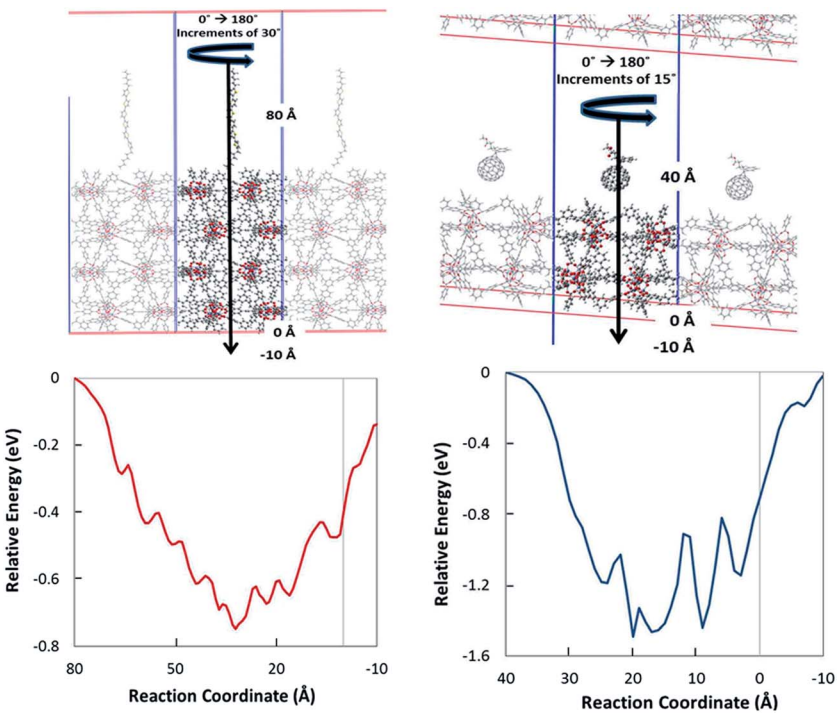

Fig. 4 (a) Schematics showing the infiltration of MOF-177 with DH6T (left) and PCBM (right). (b) Potential energy curves of the infiltration process with DH6T (left) and PCBM (right) determined at the SCC-DFTB level of theory. The reaction coordinate corresponds to the distance between the bottom of the unit cell and the center-of-mass of DH6T or PCBM.

Experimental results

DH6T and PCBM infiltration

Immersing MOF-177 crystals (Fig. 1) in saturated chlorobenzene solutions containing DH6T, PCBM, and mixtures of the two molecules produces rapid, visually discernable color changes after a few hours of exposure. This contrasts with the report by Chae *et al.*, in which infiltration with C_{60} was reported to occur after one week,[29] and is most likely due to the higher solubility of PCBM relative to C_{60}. After one week, the translucent, colorless MOF crystals immersed in the DH6T solution become pale yellow, while those exposed to PCBM become dark violet. PXRD of MOF-177 and infiltrated MOF-177 (ESI, Fig. S3†) shows no changes to the framework or the presence of new phases, indicating that the framework maintains its integrity in the presence of DH6T and PCBM. Small changes in the relative peak intensities may suggest some modification of the preferred orientation upon infiltration, but it is difficult to draw firm conclusions on this basis.

DH6T and PCBM loadings were quantified using both UV-vis spectroscopy (ESI, Fig. S4†) and elemental analysis. We obtained a DH6T content of ~0.1 wt%, corresponding to ~1 DH6T molecule for every 11 unit cells, and a PCBM loading of 22 wt%, corresponding to 2–3 PCBM molecules per unit cell. When exposed to an equimolar mixture of DH6T and PCBM, the loadings were ~0.04 wt% for DH6T and ~11 wt% for PCBM, corresponding to one DH6T molecule per 28 unit cells and 1 PCBM molecule per unit cell. Although these PCBM loadings are high (comparable to those used in PCBM-polymer blends used for bulk heterojunction devices), there is no evidence for a luminescence peak at ~500 nm exhibited by PCBM films,[40] suggesting that the post-infiltration washing procedure effectively removes any residual PCBM on the surface of the crystals. The low DH6T loading can be attributed to the linear backbone and rigidity of the DH6T molecule. Elemental analysis reported a 0.1 sulfur wt% on DH6T@MOF-177, 58.5 carbon wt% on PCBM@MOF-177, and <0.005 sulfur wt% in DH6T + PCBM@MOF-177 (ESI, Table S1†). The loadings using UV-vis spectroscopy and elemental analysis are consistent with one another.

We find that shorter thiophene oligomers also penetrate the MOF, but the loadings clearly illustrate the steric constraints imposed by the MOF-177 pore dimensions relative to the kinetic diameter and further side groups on the parent chain of an infiltrating molecule. The elemental analysis results of terthiophene (3T) and quarterthiophene (DH-4T) infiltrated MOF-177 crystals report a sulfur content of <0.005 wt% for 3T@MOF-177 and 1.25 ± 0.02 wt% for DH-4T@MOF-177. These loading contents correspond to less than one 3T molecule in a unit cell and three DH-4T molecules per unit cell. We attribute the lower loading of 3T in MOF-177 compared to both DH-4T and DH6T to steric hindrance by the alkyl side chains on DH-4T and DH6T with the MOF framework.

Luminescence spectroscopy

The emission spectrum of DH6T@MOF-177 excited within the MOF-177 excitation spectrum (345 nm) exhibits quenching of the linker-associated emission and the simultaneous appearance of a weak, broad emission band at lower energy (450–700 nm; Fig. 5a). Small shifts to shorter wavelength (~16 nm) in both the excitation and emission maxima relative to uninfiltrated MOF-177 suggest that the linker environment is modified by the presence of DH6T molecules within the framework. Both are blue shifted relative to H_3BTB in DMF, for which λ_{em} is 390 nm (Fig. 3). Hypsochromic shifts are consistent with a less polar environment within the MOF pores compared with DMF.[41]

These results demonstrate that fluorescence resonance energy transfer (FRET) occurs from the framework linker groups to DH6T. Spectral overlap between the MOF-177 emission and DH6T and PCBM absorbance is a requirement for efficient FRET to occur between emitting and absorbing molecules; this clearly exists for all three guest@MOF-177 samples (Fig. 6). The weak band at lower energy in the emission spectrum of DH6T@MOF-177 corresponds to the emission of DH6T, excited by pumping the absorption of the BTB linkers. In the solid state, the emission spectrum of DH6T (overlaid in Fig. 5a) shows a λ_{em} maximum at 512 nm and vibronic structure attributed to coupling with the C=C stretching mode[42] at 460 and 548 nm. The same structure is evident in the DH6T@MOF-177 spectrum. Similar quenching is observed when the linker and DH6T are present in solution

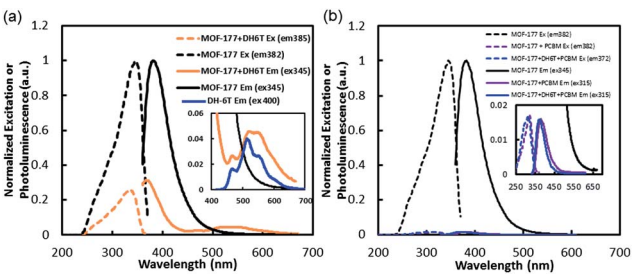

Fig. 5 Photoluminescence spectra of (a) solid state MOF-177 and DH6T@MOF-177; DH6T emission (blue curve) and (b) solid state MOF-177, PCBM@MOF-177, and DH6T + PCBM@MOF-177.

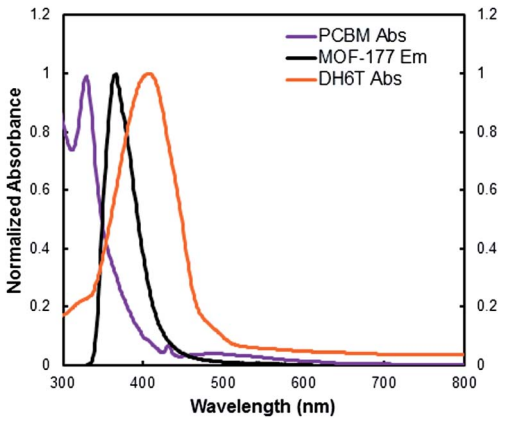

Fig. 6 Spectral overlap of MOF-177 emission (neat powder) with DH6T and PCBM absorption (dilute solutions in chlorobenzene).

(Fig. S5a†). The magnitude of the H_3BTB quenching in solution increases as the concentration of DH6T increases, as does the DH6T emission intensity; the isosbestic point shows that the two are correlated. These results not only confirm that energy transfer occurs between the H_3BTB linker and DH6T, but also that DH6T must be present as guest molecules within the MOF pores. FRET is not typically effective at distances >10 nm (discussed below), which is far shorter than the typical crystallite size in these samples (~100–200 μm).

Infiltration of MOF-177 with PCBM also quenches the MOF emission (Fig. 5b). Since no emission from PCBM is observed, however, it is not immediately clear whether this is due to non-emissive fluorescence quenching or energy transfer. However, the very strong overlap between the MOF-177 emission and the absorption by PCBM makes it very likely that FRET is occurring. A shift of the excitation spectrum to shorter wavelength is observed here as well, which may indicate that PCBM modifies electronic interactions with the linkers that stabilize the emitting excited state. The presence of both DH6T and PCBM in the MOF leads to an emission spectrum similar to PCBM@MOF-177, as seen in Fig. 5b.

Lifetime measurements and FRET properties

Decreased luminescence decay time constants show that quenching in all three guest@MOF systems is caused by interactions between the linker excited state and the quenching guest molecule and not by the formation of a ground-state complex between the linker and guest. Diffuse reflectance spectra of the infiltrated materials do not indicate the formation of a ground state guest–linker complex (Fig. S2†), confirming that Dexter energy transfer is not active here. Luminescence decay curves obtained from lifetime measurements of MOF-177 and guest@MOF-177 (ESI, Fig. S6†) were fitted to bi-exponential expressions for DH6T@MOF-177 and PCBM@MOF-177 and a tri-exponential expression for DH6T + PCBM@MOF-177 (Table 1). Both the average lifetime (τ_{avg}) of the MOF-177 PL and the individual component lifetimes decrease upon infiltration with DH6T, PCBM, and (DH6T + PCBM).

Distances for effective energy transfer and average donor–acceptor distances computed from the quenching data show that FRET is required to account for the quenching extents observed here. The Förster radii R_0 are 39 Å and 27 Å for DH6T and PCBM, respectively, which were determined from the measured MOF-177 quantum efficiency Φ_d (24.3%) and spectral overlap J. Using these values and τ_{avg} for MOF-177 and its infiltrated versions, we computed energy transfer rate constants (k_T), quantum yields (φ_{eng}), and donor–acceptor distances r (Table 2).[41] For DH6T@MOF-177, φ_{eng} is 37%; PCBM is an even more effective quencher of MOF-177 luminescence, with a φ_{eng} of 65%. Not surprisingly, infiltrating with both DH6T and PCBM results in the highest quenching, with φ_{eng} of 88%. The corresponding energy transfer rates k_T (eqn S4; see ESI†) are 2.6×10^7 s^{-1} for DH6T@MOF-177 and 8.2×10^7 s^{-1} for PCBM@MOF-177. The distances r at which these quenching extents occur are ~43 Å for DH6T and 24 Å for PCBM and are nearly the same as the Förster radii.

Table 2 Energy transfer quantities computed from steady-state luminescence decay curves

	τ_{avg} guest@MOF/τ_{avg} MOF		
	DH6T@MOF-177[a]	PCBM@MOF-177[a]	(DH6T + PCBM)@MOF-177[b]
J value (cm^6)	2.5×10^{-14}	2.7×10^{-15}	—
R (Å)	39	27	—
φ_{eng} (%)	36	66	88
k (s^{-1})	2.6×10^7	8.2×10^7	—
r (Å)	43	24	—

[a] Computed using PhotochemCAD. [b] Computed from eqn (8) in the ESI;† PhotochemCAD cannot compute quantities for three-component luminescent systems.

Discussion

Energy transfer pathways

The luminescence results described above establish that FRET is responsible for the observed quenching rates in DH6T-infiltrated MOF-177, which is likely also the case for PCBM@MOF-177. In contrast with collisional quenching processes that occur in solution, the MOF strongly immobilizes guest molecules within the pores, which can then interact with only a limited number of linkers in their immediate vicinity. Relaxed geometries for DH6T@MOF-177 and PCBM@MOF-177 predicted by DFTB indicate that the closest interatomic distances are 3.6 Å and 3.5 Å, respectively, which are close enough for interaction between their electron clouds that could produce non-radiative energy transfer (*i.e.* charge transfer). Such interactions fall off exponentially with distance, however.[41] Thus, energy transfer must occur over longer distances (>10 Å) in guest@MOF-177 materials to achieve the observed quenching levels. It is clear that this occurs for DH6T@MOF-177, for which the loading is very low, ~1 DH6T molecule per 11 unit cells. The greatest distance to any linker in a cube of 11 unit cells is 64 Å, which is significantly larger than the 39 Å Förster radius. This is consistent with the measured quenching quantum yield of 37% (Table 2). At the higher loading in PCBM@MOF-177, ~2.5 PCBM per unit cell, the maximum linker-PCBM distance is only ~15 Å, which is well within the 27 Å Förster radius. Notably, the PCBM@MOF-177 loading here (22 wt%) is comparable to typical PCBM loadings in polymer–fullerene blends (~20 wt%), where energy transfer is dominated by fluorescence resonance energy transfer (FRET) at loadings of 20 wt%.[3] However, this is achieved without phase segregation prevalent in bulk heterojunctions that increases the exciton diffusion distance.[3]

These results also suggest the possibility that some of the quenching observed in the DH6T + PCBM@MOF-177 system is due to a "FRET cascade," in which MOF-177 is the donor, PCBM is the acceptor (Fig. 7). This process (*i.e.* MOF-177 → DH6T → PCBM) consists of multiple individual FRET processes from MOF-177 → DH6T, DH6T → PCBM, and MOF-177 → PCBM. Thus, DH6T would play a dual role, serving as an acceptor for MOF-177 and a donor for PCBM and facilitating the energy

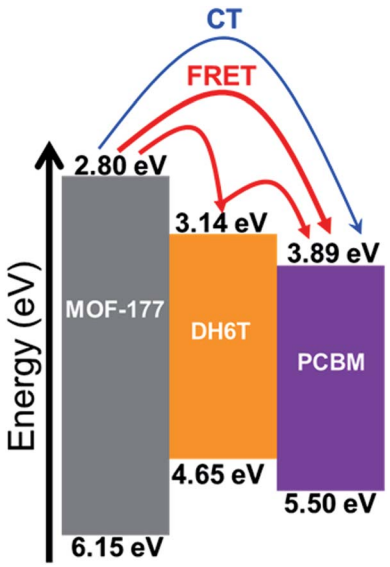

Fig. 7 MOF-177, DH6T, & PCBM band alignment predicted by SCC-DFTB.

transfer. The broad emission at longer wavelengths corresponding to DH6T, which was previously observed in DH6T@MOF-177, is absent in DH6T + PCBM@MOF-177, consistent with PCBM quenching the emission of DH6T and energy transfer from DH6T to PBCM. This mechanism is feasible in DH6T + PCBM@MOF-177 because of favorable spectral overlap between the donor (linker) emission and the absorption spectrum of the acceptors. Band gaps obtained from periodic SCC-DFTB calculations of MOF-177 and the isolated guest molecules show that there is sufficient excitation energy within the MOF linker and appropriate band alignment to enable FRET with both DH6T and PCBM (Fig. 7). As a consequence, MOF-177 is not merely a passive host for guest molecules, but plays an active role in this infiltrated system by harvesting additional photons from the solar spectrum that are efficiently transferred to DH6T and PCBM. A detailed assessment of the importance of a FRET cascade is outside the scope of this paper, however.

A remaining question concerns the origin of the multi-exponential luminescence decays produced by both MOF-177 and the guest@MOF-177 samples. The τ_1 of MOF-177 (24 ns) can be assigned to emission from individual linkers, since it closely resembles that of H_3BTB in dilute solution (21 ns) and the excitation and emission spectra are nearly identical (Fig. 3). This indicates that, within the MOF-177 structure, a given linker is largely isolated from others in the framework. However, the presence of a second, fast component with τ_0 of 10 ns indicates that additional interactions exist. The origin of this component is unclear, but possibilities include interlinker interactions, a distribution of occupied and unoccupied sites in these infiltrated MOFs, and, as was previously suggested for a porphyrin MOF system, exciton–exciton annihilation.[18]

Charge transfer

The possibility that charge transfer occurs in these guest@MOF systems cannot be completely ruled out, since this mechanism is not fully probed by our techniques. The spectral overlap between MOF-177 and DH6T, the observed luminescence quenching, and the favorable DH6T-PCBM band alignment could promote charge separation between these two molecules. These alone are not sufficient to demonstrate that it occurs here, however.

We therefore assessed the potential that charge–transfer between the MOF linker (H_3BTB), DH6T, and PCBM could occur by using TDDFT (wB97XD/6-31G(d,p)) calculations to predict the optical absorption spectra and electron density difference maps (EDDMs[43] also known as the charge difference density (CDD) maps) between various excitations. This approach is similar to that used previously to identify a CT band in another zinc based MOF.[44] The optical absorption spectra of the two donor–acceptor clusters H_3BTB@DH6T and H_3BTB@PCBM, considering the first 100 excited states, are shown in Fig. 8. In addition, EDDMs for several of the excited state transitions with

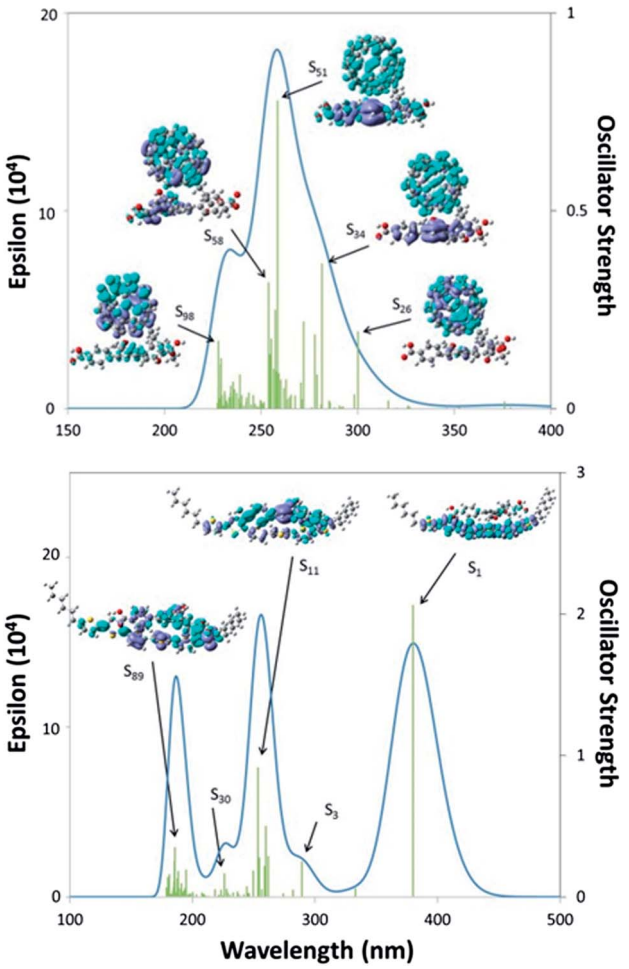

Fig. 8 Optical absorption spectra of H_3BTB/PCBM (top) and H_3BTB/DH6T (bottom) computed using TDDFT at the wB97xD/6-31G(d,p) level of theory. The molecular images show the change in electron density upon excitation. The purple and light blue regions represent a decrease (holes) and increase (electrons) in the electron density respectively. For clarity, S_3 and S_{30} transitions have been omitted. All EDDMs plots were constructed using the same isosurface contour value.

appreciable oscillator strengths are shown as inserts. EDDMs visually represent electron transfer effects upon excitation, which is determined by subtracting the ground state electron density from the excited state. These calculations show that the introduction of PCBM to create H_3BTB@PCBM leads to the formation of linker-to-guest charge transfer states. This is evident in several of the dominant optically active excited states (S_{34} and S_{51}) in the 300–250 nm spectral region (Fig. 8 top). For these transitions, the EDDMs show increased electron density on the PCBM molecule upon excitation, as represented by the light blue lobes. The purple regions represent decreased electron density and are absent on PCBM, giving evidence that charge transfer can occur.

In contrast, charge transfer states are not clearly evident in the H_3BTB@DH6T cluster, based on the EDDM analysis of several of the optically active transitions. Here, the change in electron density is either localized on the individual molecules or evenly distributed across both molecules. However, the LUMO of H_3BTB lies above that of DH6T, which implies that upon excitation of H_3BTB, charge transfer to DH6T should be feasible. These results and those for PCBM@MOF-177 indicate direct parallels between guest@MOF systems and conventional bulk heterojunctions, in that proper composition of the linker group and guest molecular orbitals, as well as their energy alignment, are needed to enable charge transfer.

Conclusions

The results presented here indicate that MOFs can function as hosts for organic donor and acceptor molecules typical of those used in excitonic devices, such as bulk heterojunctions and solid-state lighting. The spectroscopy of DH6T and PCBM confined within MOF-177 indicates that efficient quenching of the MOF-177 luminescence by FRET occurs, which recent work indicates is an important, possibly dominant, mechanism of energy transfer in polymer–fullerene blends.[3] Although the nature of their constituents and bonding makes most MOFs nominally insulators, even these can play an active role by serving as a photon antenna to harvest light that is not efficiently absorbed by the donor and transfer it to guest acceptor molecules. Our results suggest that, by taking full advantage of MOF porosity, as well as their inherent structural order, one can create MOF–donor–acceptor hybrids in which all constituents play an active role. This not only allows the chemical environment of the donor and acceptor molecules to be clearly defined, it also enables the use of accurate first-principles theoretical methods that would be difficult to implement in disordered polymeric systems. By way of illustration, TDDFT calculations presented here indicate that some PCBM@MOF-177 excited states involve linker-to-guest charge transfer, suggesting that photoconductivity might be achievable in an appropriately designed guest@MOF system.

Acknowledgements

This work was supported by the U.S. Department of Energy Office of Energy Efficiency and Renewable Energy SunShot Program under award number DE-FOA-0000387-1923 and Sandia National Laboratories' Laboratory Directed Research and Development (LDRD) Program. SEM imaging was performed at the Molecular Foundry, Lawrence Berkeley National Laboratory, supported by the Office of Science, Office of Basic Energy Sciences of the U.S. Department of Energy under Contract no. DE-AC02-05CH11231. The authors are grateful to Prof. Jeffrey Long and Brian Weirs (UC Berkeley Dept. of Chemistry) for the use of their UV-vis/diffuse reflectance instrument. Sandia National Laboratories is a multi-program laboratory managed and operated by Sandia Corporation, a wholly owned subsidiary of Lockheed Martin Corporation, for the U.S. Department of Energy's National Nuclear Security Administration under contract DE-AC04-94AL85000.

References

1 R. A. J. Janssen and J. Nelson, *Adv. Mater.*, 2013, **25**, 1847–1858.
2 Y.-X. Liu, M. A. Summers, S. R. Scully and M. D. McGehee, *J. Appl. Phys.*, 2006, **99**, 093521–093524.
3 A. J. Ward, A. Ruseckas and I. D. W. Samuel, *J. Phys. Chem. C*, 2012, **116**, 23931–23937.
4 T. Kirchartz, K. Taretto and U. Rau, *J. Phys. Chem. C*, 2009, **113**, 17958–17966.
5 W. U. Huynh, J. J. Dittmer and A. P. Alivisatos, *Science*, 2002, **295**, 2425–2427.
6 S. E. Shaheen, C. J. Brabec, N. S. Sariciftci, F. Padinger, T. Fromherz and J. C. Hummelen, *Appl. Phys. Lett.*, 2001, **78**, 841–843.
7 M. M. Wienk, J. M. Kroon, W. J. H. Verhees, J. Knol, J. C. Hummelen, P. A. van Hal and R. A. J. Janssen, *Angew. Chem., Int. Ed.*, 2003, **42**, 3371–3375.
8 Y. Yi, V. Coropceanu and J.-L. Breédas, *J. Am. Chem. Soc.*, 2009, **131**, 15777–15783.
9 P. Peumans, S. Uchida and S. R. Forrest, *Nature*, 2003, **425**, 158–162.
10 L. Schmidt-Mende, A. Fechtenkötter, K. Müllen, E. Moons, R. H. Friend and J. D. MacKenzie, *Science*, 2001, **293**, 1119–1122.
11 B. C. Thompson and J. M. J. Fréchet, *Angew. Chem., Int. Ed.*, 2008, **47**, 58–77.
12 G. Ferey, *Chem. Soc. Rev.*, 2008, **37**, 191–214.
13 H. Li, M. Eddaoudi, M. O'Keeffe and O. M. Yaghi, *Nature*, 1999, **402**, 276–279.
14 J.-R. Li, R. J. Kuppler and H.-C. Zhou, *Chem. Soc. Rev.*, 2009, **38**, 1477–1504.
15 R. Banerjee, H. Furukawa, D. Britt, C. Knobler, M. O'Keeffe and O. M. Yaghi, *J. Am. Chem. Soc.*, 2009, **131**, 3875–3877.
16 Y. Cui, Y. Yue, G. Qian and B. Chen, *Chem. Rev.*, 2011, **112**, 1126–1162.
17 M. Eddaoudi, J. Kim, N. Rosi, D. Vodak, J. Wachter, M. O'Keeffe and O. M. Yaghi, *Science*, 2002, **295**, 469–472.
18 H.-J. Son, S. Jin, S. Patwardhan, S. J. Wezenberg, N. C. Jeong, M. So, C. E. Wilmer, A. A. Sarjeant, G. C. Schatz, R. Q. Snurr, O. K. Farha, G. P. Wiederrecht and J. T. Hupp, *J. Am. Chem. Soc.*, 2012, **135**, 862–869.

19 H. Khajavi, J. Gascon, J. M. Schins, L. D. A. Siebbeles and F. Kapteijn, *J. Phys. Chem. C*, 2011, **115**, 12487–12493.

20 L.-M. Yang, P. Ravindran, P. Vajeeston and M. Tilset, *J. Mater. Chem.*, 2012, **22**, 16324–16335.

21 M. Fuentes-Cabrera, D. M. Nicholson, B. G. Sumpter and M. Widom, *J. Chem. Phys.*, 2005, **123**, 124713–124715.

22 J. Gascon, M. D. Hernández-Alonso, A. R. Almeida, G. P. M. van Klink, F. Kapteijn and G. Mul, *ChemSusChem*, 2008, **1**, 981–983.

23 M. D. Allendorf, C. A. Bauer, R. K. Bhakta and R. J. T. Houk, *Chem. Soc. Rev.*, 2009, **38**, 1330–1352.

24 C. A. Kent, D. Liu, T. J. Meyer and W. Lin, *J. Am. Chem. Soc.*, 2012, **134**, 3991–3994.

25 C. A. Kent, B. P. Mehl, L. Ma, J. M. Papanikolas, T. J. Meyer and W. Lin, *J. Am. Chem. Soc.*, 2010, **132**, 12767–12769.

26 C. Wang and W. Lin, *J. Am. Chem. Soc.*, 2011, **133**, 4232–4235.

27 S. Jin, H.-J. Son, O. K. Farha, G. P. Wiederrecht and J. T. Hupp, *J. Am. Chem. Soc.*, 2013, **135**, 955–958.

28 H. C. Streit, M. Adlung, O. Shekhah, X. Stammer, H. K. Arslan, O. Zybaylo, T. Ladnorg, H. Gliemann, M. Franzreb, C. Woll and C. Wickleder, *Chemphyschem*, 2012, **13**, 2699–2702.

29 H. K. Chae, D. Y. Siberio-Perez, J. Kim, Y. Go, M. Eddaoudi, A. J. Matzger, M. O'Keeffe and O. M. Yaghi, *Nature*, 2004, **427**, 523–527.

30 D. Porezag, T. Frauenheim, T. Köhler, G. Seifert and R. Kaschner, *Phys. Rev. B: Condens. Matter Mater. Phys.*, 1995, **51**, 12947–12957.

31 G. Seifert, D. Porezag and T. Frauenheim, *Int. J. Quantum Chem.*, 1996, **58**, 185–192.

32 M. Elstner, D. Porezag, G. Jungnickel, J. Elsner, M. Haugk, T. Frauenheim, S. Suhai and G. Seifert, *Phys. Rev. B: Condens. Matter Mater. Phys.*, 1998, **58**, 7260–7268.

33 N. H. Moreira, G. Dolgonos, B. l. Aradi, A. L. da Rosa and T. Frauenheim, *J. Chem. Theory Comput.*, 2009, **5**, 605–614.

34 B. Aradi, B. Hourahine and T. Frauenheim, *J. Phys. Chem. A*, 2007, **111**, 5678–5684.

35 J.-D. Chai and M. Head-Gordon, *Phys. Chem. Chem. Phys.*, 2008, **10**, 6615–6620.

36 G. W. T. M. J. Frisch, H. B. Schlegel, G. E. Scuseria, M. A. Robb, J. R. Cheeseman, G. Scalmani, V. Barone, B. Mennucci, G. A. Petersson, H. Nakatsuji, M. Caricato, X. Li, H. P. Hratchian, A. F. Izmaylov, J. Bloino, G. Zheng, J. L. Sonnenberg, M. Hada, M. Ehara, K. Toyota, R. Fukuda, J. Hasegawa, M. Ishida, T. Nakajima, Y. Honda, O. Kitao, H. Nakai, T. Vreven, J. A. Montgomery, Jr., J. E. Peralta, F. Ogliaro, M. Bearpark, J. J. Heyd, E. Brothers, K. N. Kudin, V. N. Staroverov, R. Kobayashi, J. Normand, K. Raghavachari, A. Rendell, J. C. Burant, S. S. Iyengar, J. Tomasi, M. Cossi, N. Rega, J. M. Millam, M. Klene, J. E. Knox, J. B. Cross, V. Bakken, C. Adamo, J. Jaramillo, R. Gomperts, R. E. Stratmann, O. Yazyev, A. J. Austin, R. Cammi, C. Pomelli, J. W. Ochterski, R. L. Martin, K. Morokuma, V. G. Zakrzewski, G. A. Voth, P. Salvador, J. J. Dannenberg, S. Dapprich, A. D. Daniels, Ö. Farkas, J. B. Foresman, J. V. Ortiz, J. Cioslowski and D. J. Fox, Gaussian, Inc., Wallingford CT, 2009.

37 A. R. Millward and O. M. Yaghi, *J. Am. Chem. Soc.*, 2005, **127**, 17998–17999.

38 J. J. Perry Iv, P. L. Feng, S. T. Meek, K. Leong, F. P. Doty and M. D. Allendorf, *J. Mater. Chem.*, 2012, **22**, 10235–10248.

39 C. A. Bauer, T. V. Timofeeva, T. B. Settersten, B. D. Patterson, V. H. Liu, B. A. Simmons and M. D. Allendorf, *J. Am. Chem. Soc.*, 2007, **129**, 7136–7144.

40 S. Cook, H. Ohkita, Y. Kim, J. J. Benson-Smith, D. D. C. Bradley and J. R. Durrant, *Chem. Phys. Lett.*, 2007, **445**, 276–280.

41 J. R. Lakowicz, *J. Biomed. Opt.*, 2008, **13**, 029901.

42 A. Yassar, G. Horowitz, P. Valet, V. Wintgens, M. Hmyene, F. Deloffre, P. Srivastava, P. Lang and F. Garnier, *J. Phys. Chem.*, 1995, **99**, 9155–9159.

43 M. Sun, *J. Chem. Phys.*, 2006, **124**, 054903.

44 B. D. McCarthy, E. R. Hontz, S. R. Yost, T. Van Voorhis and M. Dinca, *J. Phys. Chem. Lett.*, 2013, **4**, 453–458.